PHYSICAL REVIEW A **92**, 031802(R) (2015)

Optomechanical Raman-ratio thermometry

T. P. Purdy,[1,2,*] P.-L. Yu,[1,2] N. S. Kampel,[1,2] R. W. Peterson,[1,2] K. Cicak,[3] R. W. Simmonds,[3] and C. A. Regal[1,2,†]
[1]*JILA, University of Colorado and National Institute of Standards and Technology, Boulder, Colorado 80309-0440, USA*
[2]*Department of Physics, University of Colorado, Boulder, Colorado 80309, USA*
[3]*National Institute of Standards and Technology, Boulder, Colorado 80305, USA*
(Received 27 June 2014; revised manuscript received 29 June 2015; published 9 September 2015)

The temperature dependence of the asymmetry between Stokes and anti-Stokes Raman scattering can be exploited for self-calibrating, optically based thermometry. In the context of cavity optomechanics, we observe the cavity-enhanced scattering of light interacting with the standing-wave drumhead modes of a Si_3N_4 membrane mechanical resonator. The ratio of the amplitude of Stokes to anti-Stokes scattered light is used to measure temperatures of optically cooled mechanical modes, down to the level of a few vibrational quanta. We demonstrate that the Raman-ratio technique allows the measurement of the physical temperature of our device over a range extending from cryogenic temperatures to within an order of magnitude of room temperature.

DOI: 10.1103/PhysRevA.92.031802 PACS number(s): 42.50.Wk, 42.65.−k

Raman light scattering has proven to be a robust and powerful technique for *in situ* thermometry. Many material-specific properties governing Raman transitions, such as the Stokes shift, spectral linewidth, and scattering rate vary with temperature. However, for any Raman system the ratio of spontaneously scattered Stokes versus anti-Stokes photons is a direct measure of the initial population of the motional state. For example, at zero temperature the process of anti-Stokes scattering, which attempts to lower the motional state below the ground state, is entirely suppressed; whereas the Stokes scattering, which raises the motional state, is allowed. For thermally occupied states, an absolute, self-calibrating temperature measurement is possible by measuring this asymmetry in Raman scattering. Distributed optical fiber sensors [1] and solid state systems [2–4] make use of spontaneous Raman scattering between optical phonon levels for temperature measurements, and combustion chemistry diagnostics use rotational-vibrational molecular levels in a similar fashion [5].

In principle, Raman scattering from any mechanical degree of freedom in a solid-state environment has the potential to provide local temperature measurements, but for low-frequency micromechanical resonances, this is a considerable challenge. Recent experiments in the field of quantum cavity optomechanics [6–8] have used cavity enhancement to collect Raman-scattered light from localized acoustic resonances and demonstrate a Stokes/anti-Stokes asymmetry. However, the potential for using this asymmetry to perform absolute, self-calibrated thermometry remains relatively unexplored. Here we measure the asymmetry of Raman scattering in a membrane-in-cavity optomechanical system (Fig. 1) over a wide range of physical temperatures between 4.8 and 50 K. We find agreement with conventional thermometry over this range to within 10%, and we discuss the sensitivity of the measurement to a variety of parameters.

In our optomechanical system, the motional states are the megahertz frequency vibrational levels of a membrane mechanical resonator, and an optical resonance is provided by an optical cavity surrounding the membrane. Departing from previous measurement schemes [6,8], the Stokes and anti-Stokes peaks are simultaneously derived from a single, resonant laser tone. The Raman asymmetry becomes more pronounced in certain mechanical normal modes of the resonator when they are optically cooled near their ground state with a separate laser tone. We are able to realize a damped displacement spectral density near the membrane resonance frequency equal to that expected from a resonator with an effective temperature as low as 150 μK ($\bar{n} \sim 2$ vibrational quanta) [9–12]. We then measure the physical temperature of our device by extrapolating the Raman sideband asymmetry to zero optical damping.

Raman-ratio thermometry is based on the idea that at a finite temperature the ground state manifold of the Raman levels is occupied according to a well-understood statistical weighting. The ratio of Stokes to anti-Stokes Raman transitions is equal to $R_{sa} = e^{\hbar\omega_m/k_bT} = (\bar{n}+1)/\bar{n}$, where ω_m is the mechanical resonance frequency and T is the temperature [13,14]. The spectrum of Raman scattered light transmitted through an optomechanical cavity [Fig. 1(b)] is given by

$$S(\omega) \propto \frac{\bar{n}}{\left(\frac{\Gamma_m}{2}\right)^2 + (\omega_m - \omega)^2} + \frac{\bar{n}+1}{\left(\frac{\Gamma_m}{2}\right)^2 + (\omega_m + \omega)^2}.$$

This expression holds when the laser is resonant with the optical cavity, and the optical cavity linewidth is much larger than the mechanical linewidth Γ_m. The first (second) term corresponds to the anti-Stokes (Stokes) scattering peak shifted by ω_m ($-\omega_m$) from the input laser frequency, and ω is the frequency relative to the input laser frequency. Taking the ratio of the amplitude of the Stokes and anti-Stokes peaks directly yields the mechanical occupation, $\bar{n} = 1/(R_{sa} - 1)$.

Our membrane-in-cavity optomechanical system [15] consists of a high-tensile-stress, silicon nitride membrane in the standing wave of a Fabry-Perot optical resonator [16] [Fig. 1(a)]. The system is operated in a helium flow cryostat, with a temperature, T_0, that is set in the range of 4.8–50 K. The mechanical modes that couple to the optical resonance are those of a square drum described by mode indices (m,n), which count the number of antinodes along each axis of the square. We have employed two devices for our measurements.

*Present address: NIST, Gaithersburg, MD 20899; thomas.purdy@nist.gov
†regal@colorado.edu

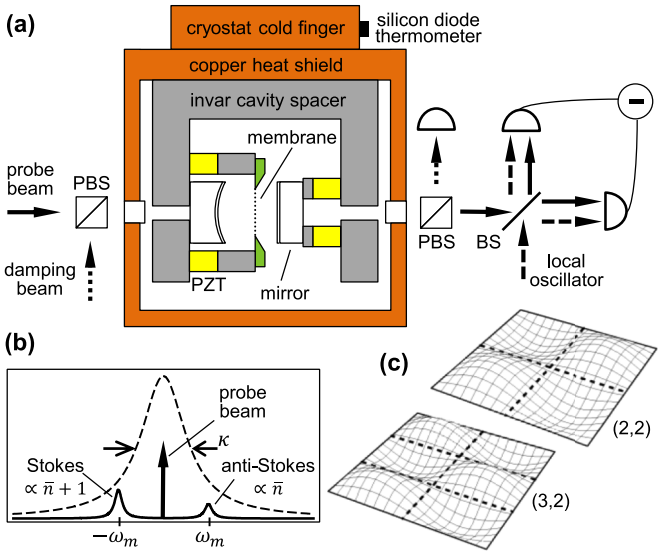

FIG. 1. (Color online) Optomechanical Raman-ratio thermometry. (a) Two orthogonally polarized laser beams are coupled into a cryogenic membrane-in-cavity optomechanical system. Raman scattered light from the resonant probe beam is analyzed with balanced heterodyne detection. The red detuned damping beam Raman sideband cools membrane motion [Beam splitter (BS), polarizing beam splitter (PBS), and piezoelectric transducer (PZT)]. (b) The spectrum of transmitted probe beam light shows Raman scattering peaks shifted by $\pm\omega_m$, where ω_m is the mechanical resonance frequency. The asymmetry in the spectral peaks, dependent on the effective thermal occupation of the mechanical mode, forms the basis for a self-calibrating thermometer. Also indicated is the spectral response of the optical cavity (dashed curve). (c) Spatial profile of the (2,2) and (3,2) drumhead mode of the membrane.

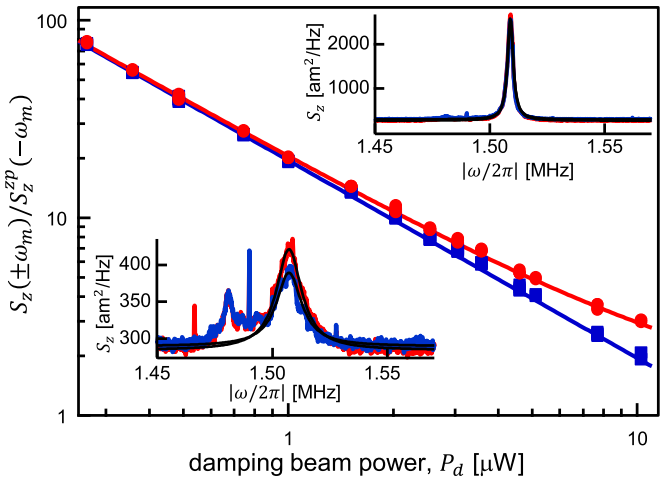

FIG. 2. (Color online) Peak amplitude of Stokes $S_z(-\omega_m)$ (red circles) and anti-Stokes $S_z(+\omega_m)$ (blue squares) Raman peaks of the (2,2) mode. Spectral densities are expressed in units of mode displacement. The scale $S_z^{zp}(-\omega_m) = S_z(-\omega_m)|_{\bar{n}=0}$ corresponds to one quanta of vibrational motion. The solid red and blue lines are fits. The statistical error is smaller than the size of the markers. $P_p = 5$ μW and $\kappa/2\pi = 1.8$ MHz. The upper (lower) inset shows the Raman spectra for $P_d = 1.5$ μW (7.7 μW), along with Lorentzian fits (including only the frequency range above ~1.50 MHz) in black. Noise from thermally occupied mechanical modes of the substrate is visible from 1.47 to 1.50 MHz. The sharp features at 1.46 and 1.49 MHz are electromagnetic interferences.

The data shown in Figs. 2 and 3(a) focus on the (2,2) mode of a 500-μm square by 40-nm-thick membrane, with resonance frequency $\omega_m^{(2,2)}/2\pi = 1.509$ MHz and intrinsic linewidth $\Gamma_0^{(2,2)}/2\pi = 0.46$ Hz. The data shown in Figs. 3(b) and 4 are primarily from the (3,2) mode of a 375-μm square by 100-nm-thick membrane, $\omega_m^{(3,2)}/2\pi = 2.637$ MHz, $\Gamma_0^{(3,2)}/2\pi = 0.84$ Hz, which is supported by a silicon substrate patterned into a square-lattice phononic crystal (device A of Ref. [17]). The acoustic band structure is engineered to provide a gap in the substrate mechanical mode density around the (3,2) mode, which diminishes noise from thermally occupied modes of the substrate [17,18].

The optical cavity consists of two mirrors separated by 3.5 mm, each with 10^{-4} fractional transmission. The optical linewidth, κ, is dependent on the location of the membrane in the cavity [19], and is on the order of a few megahertz. Optomechanical coupling is achieved as the optical resonance frequency is modulated by the displacement of the vibrating membrane along the optical standing wave. This interaction is characterized by a single photon coupling rate of $g_0^{(2,2)}/2\pi = 33$ Hz for the data in Fig. 2 or $g_0^{(3,2)}/2\pi = 18$ Hz for the data in Fig. 4. The cavity is driven with two orthogonally polarized laser beams derived from the same 1064 nm laser source [Fig. 1(a)] (see Supplemental Material [20]). The probe beam is actively stabilized to be resonant with the optical cavity. The transmitted Raman scattered light from this beam is analyzed with an optical heterodyne detection system. The orthogonal polarization mode is driven by the damping beam, which is tuned to a frequency lower than the optical resonance.

For the red-detuned damping beam, the anti-Stokes scattering rate is resonantly enhanced by the cavity [13,14]. Each anti-Stokes scattered photon that exits the cavity carries one vibrational quantum of energy out of the system. The mode reaches an equilibrium when the optical cooling rate is matched by the rate at which thermal excitations enter the

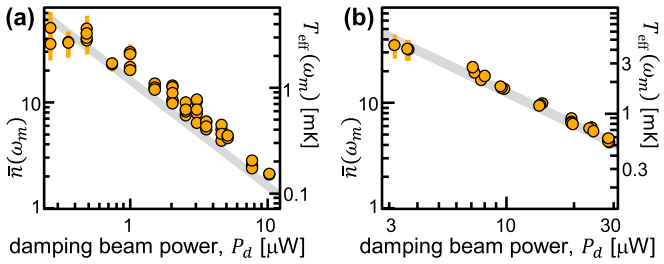

FIG. 3. (Color online) Effective mode occupation at mechanical resonance. Numerically integrating the Raman peaks over a 4 kHz span around the mechanical resonance and taking their ratio yields a measure of the mode effective temperature (orange circles) for (a) the (2,2) mode of the non-phononic-crystal device and (b) the (3,2) mode of the phononic-crystal device. Due to decreased optomechanical coupling, the (3,2) mode does not reach as low a mechanical occupation as the (2,2) mode. Gray bands are the prediction of Raman sideband cooling whose width stems from uncertainty in T_0 as measured by the diode thermometer. Vertical error bars represent estimated statistical standard deviation.

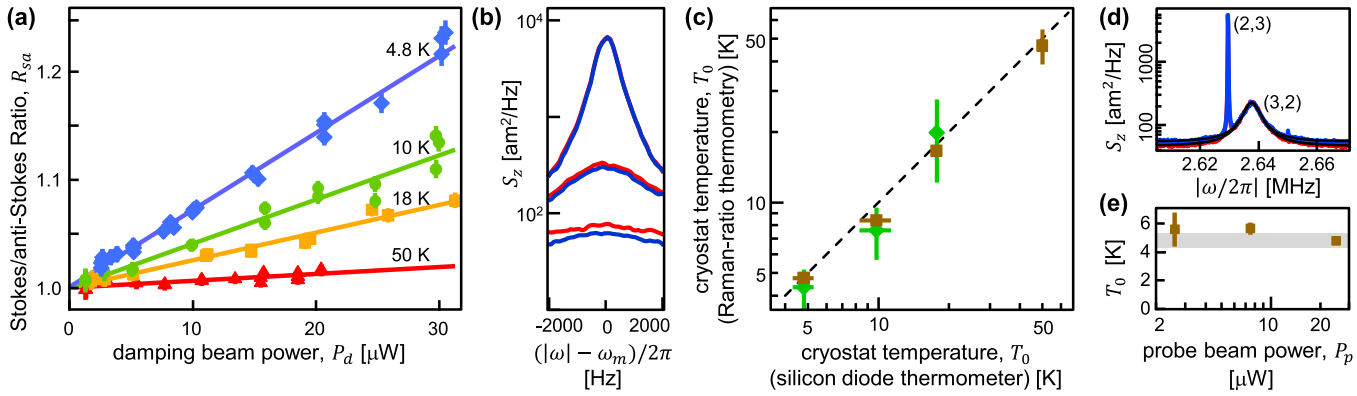

FIG. 4. (Color online) (a) Stokes–anti-Stokes peak ratio for the (3,2) mode at four cryostat temperatures. Solid curves are linear fits to the data. $P_p = 26\ \mu$W and $\kappa/2\pi = 2.7$ MHz. (b) Stokes (red) and anti-Stokes (blue) spectra near the (3,2) mode for P_d of 3.2 μW (top), 14 μW (middle), and 28 μW (bottom). Resolution bandwidth is 100 Hz. (c) Comparison of Raman-ratio thermometry with silicon diode thermometer for the (3,2) mode (brown squares) and (5,2) mode (green diamonds). The dashed line indicates agreement between the two methods. (d) Raman spectra of (2,3) and (3,2) mode at $P_d = 25\ \mu$W. Black curves are fit Lorentzians excluding the region around the (2,3) mode. (e) Extracted temperature, T_0, for various probe powers. Vertical error bars in (a), (c), and (e) represent estimated statistical standard deviation. Horizontal error bars in (c) and width of gray band in (e) represent a combination of the diode thermometer accuracy (±0.5 K) and inaccuracy introduced by drift and oscillations in the temperature over the span of the measurement.

system. The effective temperature of a mode is approximately $T_{\rm eff} = T_0 \frac{\Gamma_0}{\Gamma_m}$, in the experimentally relevant case where $\Gamma_0 \ll \Gamma_m \ll \kappa$; here Γ_m is the optically induced mechanical damping rate, and Γ_0 is the intrinsic mechanical damping rate. The cooling is more efficient when the resolved sideband parameter $\omega_m/\kappa \gg 1$. However, such a ratio will suppress the Raman peaks generated by the resonant probe beam. We build our system with $\omega_m/\kappa \sim 1$ so that we can maintain cooling efficiency and detect the Raman signals generated by one probe beam.

By varying the power of the damping beam, we are able to damp motion and reduce the effective mode temperature by up to a factor of 3×10^4. Figure 2 shows the Stokes and anti-Stokes peak amplitudes generated by the resonant probe beam as the damping beam power, P_d, is increased. The power of the transmitted probe beam, P_p, is held constant. As expected, the height of the anti-Stokes peak decreases with damping beam power as the mode is cooled. For weak damping the two Raman peaks are equal in amplitude, whereas at strongest damping the Stokes peak is 50% larger than the anti-Stokes peak as the mode approaches its quantum ground state.

To compute the effective temperature of the mode, we numerically integrate the Raman peaks over a 4 kHz span around the mechanical resonance and calculate their ratios. This narrowband analysis minimizes the effect of noise from the thermally occupied mechanical modes of the non-phononic-crystal substrate (Fig. 2, inset; e.g., 1.47–1.50 MHz) [16,17]. In addition, the mechanical occupation near the resonance is a relevant figure of merit for many applications of optomechanics, including resonant force sensing and the generation of optomechanically squeezed light [21]. The analysis indicates that the (2,2) mode reaches $\bar{n}(\omega_m) = 2.1 \pm 0.2$. We stop at this number because the extraneous noise is significant. Integrating the excess noise over the entire frequency span of Fig. 2 (inset) results in slightly less than one quantum of apparent motion. In addition, for this mode, the occupations measured over a wide range of damping beam power are systematically ∼15% larger than predicted by Raman sideband cooling. This discrepancy, which is absent in the phononic-crystal-isolated (3,2) mode [Fig. 3(b)], is likely due to the influence of substrate motion.

Ultimately, the mechanical occupation one can reliably measure with Raman-ratio thermometry is limited by the Heisenberg measurement-disturbance uncertainty principle. As we increase the probe beam power to increase the signal-to-noise ratio, the optical forces from the shot noise [radiation pressure shot noise (RPSN)] [22] will increase as well. The RPSN-driven motion set the lowest temperature one can measure. In the data of $\bar{n}(\omega_m) = 2.1$, the signal-to-noise ratio is ∼1 dB. The contribution from RPSN is 0.2 quanta.

We next consider Raman-ratio thermometry as a means to determine the physical temperature of the device. The Raman asymmetry of undamped modes is small ($\sim 10^{-4}$) and precludes directly ascertaining the physical device temperature. Nevertheless, with our ability to perform strong optomechanical cooling, we can extrapolate the temperature of the undamped membrane modes from measurements of the asymmetry as a function of optical damping [Fig. 4(a)]. The undamped occupation of the mechanical mode is given by $(dR_{sa}/dP_d)^{-1}(d\Gamma_m/dP_d)(1/\Gamma_0)$.

Here we employ a membrane resonator embedded in a phononic crystal substrate, which reduces the effects of substrate motion to a level below the statistical noise. Thermometry is performed on the (3,2) mode with the cryostat held at several different temperatures between 4.8 and 50 K. In Fig. 4(c) the extrapolated temperatures are compared to the temperature as measured by a silicon diode thermometer attached to the cryostat. The results agree within the statistical uncertainty with an average deviation of less than 10%. As an additional confirmation, we perform the same thermometry procedure on the (5,2) mode, which is also located in a phononic band gap of the substrate and find agreement with the previous measurements. However, the statistical error on the (5,2) mode measurement is much larger because the optomechanical coupling is smaller than the (3,2) mode.

Thermometry relying on sideband asymmetry does not require accurate knowledge of often-difficult-to-measure system parameters such as the optomechanical coupling rate, effective modal mass, circulating optical power, or optical detection efficiency. Additionally, the single-resonant-probe method [7] employed in this work reduces the sensitivity to many systematic errors as compared to techniques that employ multiple off-resonant probe tones [6,8]. Such effects include drift in the relative amplitude of the probes, optomechanical modification of the mechanical susceptibility, coherent optomechanically induced interference between the probes [23], and increased sensitivity to classical laser noise [24]. However, many systematic effects in our system can lead to error in temperature determination, and we now discuss several of these potential error sources.

A necessary external input parameter to extract the physical temperature is the intrinsic mechanical linewidth, which is measured via mechanical ringdown with an uncertainty of a few tenths of a percent. However, long-term drift in the mechanical linewidth can be at the percent level. The intrinsic linewidth is recorded at each cryostat temperature, and found to increase from 0.84 Hz at 4.8 K to 1.07 Hz at 50 K. The optically damped mechanical linewidths are obtained by Lorentzian fits to Raman spectra.

Heating induced by absorbed laser light can cause thermal gradients between the membrane and silicon diode thermometer and increase $\bar{n}$. We see no evidence for absorptive heating, which would cause deviations from linearity in the data of Fig. 4(a) and from the power-law fit of the anti-Stokes data of Fig. 2(a). Another, more fundamental, systematic effect is the RPSN drive motion, as discussed above. It contributes 0.2 K to T_0 for $P_p = 26\ \mu$W probing the (3,2) mode (see Supplemental Material). We apply this correction to the extracted physical temperature data in Fig. 4(c) and the theoretical expectation bands of Fig. 3.

In addition to the quantum noise of the probe beam, optomechanically mediated correlations in the classical laser noise can also lead to systematic error. Such noise-squashing or noise-cancellation effects can change the relative heights of the Raman peaks leading to an underestimate of the effective mode occupation [8,24,25]. To assess this systematic, we have independently measured the classical phase and amplitude noise as well as the detuning of the input probe beam (see Supplemental Material). These measurements constrain the potential error [24] on temperature due to classical laser noise correlations to be at the percent level or less under all operating conditions. Additionally, we have reduced the probe beam power by an order of magnitude and observed only a weak trend in extracted temperature [Fig. 4(e)], which confirms that the effects of both classical laser noise and absorptive heating are small.

The (3,2) membrane mode is nearly degenerate with the (2,3) mode, with a frequency difference between the two modes of 7.2 kHz [Fig. 4(d)]. For all values of employed optical damping the (3,2) mode and (2,3) mode are well resolved in the spectrum. For thermometry, Raman peaks are always compared within ± 2 kHz of the peak of (3,2) mode resonance. Thus we believe the presence of the (2,3) mode is a negligible perturbation on the thermometry data shown in Fig. 4. Increasing the optical damping well beyond the level presented here could cause mode hybridization and complicate the interpretation of the Raman spectra [26].

In conclusion, we have shown that Raman asymmetry is a viable technique to diagnose both the effective mode temperature of an optically damped membrane resonator and the physical temperature of the same device. These measurements demonstrate the self-calibrating nature of the method and elucidate many of the systematic uncertainties. Our results show that the quantum effects governing the asymmetry [8,27] are visible in a membrane-in-cavity optomechanical system operated within an order of magnitude of room temperature.

Note added. Recently, we became aware of parallel studies [28].

This work was supported by the DARPA QuASAR program, the ONR YIP, the AFOSR PECASE, and the National Science Foundation under Grant No. 1125844. C.R. thanks the Clare Boothe Luce Foundation for support. P.-L.Y. thanks the Taiwan Ministry of Education for support.

[1] J. P. Dakin, D. J. Pratt, G. W. Bibby, and J. N. Ross, in *Optical Fiber Sensors* (Optical Society of America, Washington, D.C., 1985), paper PDS3.

[2] T. R. Hart, R. L. Aggarwal, and B. Lax, Phys. Rev. B **1**, 638 (1970).

[3] B. J. Kip and R. J. Meier, Appl. Spectrosc. **44**, 707 (1990).

[4] J. B. Cui, K. Amtmann, J. Ristein, and L. Ley, J. Appl. Phys. **83**, 7929 (1998).

[5] A. C. Eckbreth, *Laser Diagnostics for Combustion Temperature and Species*, 2nd ed. (Gordon and Breach, Amsterdam, Netherlands, 1996), Chap. 5.

[6] A. H. Safavi-Naeini, J. Chan, J. T. Hill, Thiago P. Mayer Alegre, A. Krause, and O. Painter, Phys. Rev. Lett. **108**, 033602 (2012).

[7] N. Brahms, T. Botter, S. Schreppler, D. W. C. Brooks, and D. M. Stamper-Kurn, Phys. Rev. Lett. **108**, 133601 (2012).

[8] A. J. Weinstein, C. U. Lei, E. E. Wollman, J. Suh, A. Metelmann, A. A. Clerk, and K. C. Schwab, Phys. Rev. X **4**, 041003 (2014).

[9] F. Diedrich, J. C. Bergquist, W. M. Itano, and D. J. Wineland, Phys. Rev. Lett. **62**, 403 (1989).

[10] C. Monroe, D. M. Meekhof, B. E. King, S. R. Jefferts, W. M. Itano, D. J. Wineland, and P. Gould, Phys. Rev. Lett. **75**, 4011 (1995).

[11] P. S. Jessen, C. Gerz, P. D. Lett, W. D. Phillips, S. L. Rolston, R. J. C. Spreeuw, and C. I. Westbrook, Phys. Rev. Lett. **69**, 49 (1992).

[12] A. M. Kaufman, B. J. Lester, and C. A. Regal, Phys. Rev. X **2**, 041014 (2012).

[13] F. Marquardt, J. P. Chen, A. A. Clerk, and S. M. Girvin, Phys. Rev. Lett. **99**, 093902 (2007).

[14] I. Wilson-Rae, N. Nooshi, W. Zwerger, and T. J. Kippenberg, Phys. Rev. Lett. **99**, 093901 (2007).

[15] J. D. Thompson, B. M. Zwickl, A. M. Jayich, F. Marquardt, S. M. Girvin, and J. G. E. Harris, Nature (London) **452**, 72 (2008).

[16] T. P. Purdy, R. W. Peterson, P.-L. Yu, and C. A. Regal, New J. Phys. **14**, 115021 (2012).

[17] P.-L. Yu, K. Cicak, N. S. Kampel, Y. Tsaturyan, T. P. Purdy, R. W. Simmonds, and C. A. Regal, Appl. Phys. Lett. **104**, 023510 (2014). We note that measured mechanical resonances of all of the membrane modes are shifted lower in frequency compared to those reported in this reference. This shift moves the (3,2) resonance closer to the center of mechanical band gap. The change may be the result of a stress reduction due to differences in sample mounting technique, mass loading from surface contamination, or device aging.

[18] Y. Tsaturyan, A. Barg, A. Simonsen, L. G. Villanueva, S. Schmid, A. Schliesser, and E. S. Polzik, Opt. Express **22**, 6810 (2014).

[19] D. J. Wilson, C. A. Regal, S. B. Papp, and H. J. Kimble, Phys. Rev. Lett. **103**, 207204 (2009).

[20] See Supplemental Material at http://link.aps.org/supplemental/10.1103/PhysRevA.92.031802 for experimental details.

[21] T. P. Purdy, P.-L. Yu, R. W. Peterson, N. S. Kampel, and C. A. Regal, Phys. Rev. X **3**, 031012 (2013).

[22] T. P. Purdy, R. W. Peterson, and C. A. Regal, Science **339**, 801 (2013).

[23] S. Weis, R. Riviere, S. Deleglise, E. Gavartin, O. Arcizet, A. Schliesser, and T. J. Kippenberg, Science **330**, 1520 (2010).

[24] A. M. Jayich, J. C. Sankey, K. Borkje, D. Lee, C. Yang, M. Underwood, L. Childress, A. Petrenko, S. M. Girvin, and J. G. E. Harris, New J. Phys. **14**, 115018 (2012).

[25] A. Pontin, C. Biancofiore, E. Serra, A. Borrielli, F. S. Cataliotti, F. Marino, G. A. Prodi, M. Bonaldi, F. Marin, and D. Vitali, Phys. Rev. A **89**, 033810 (2014).

[26] A. B. Shkarin, N. E. Flowers-Jacobs, S. W. Hoch, A. D. Kashkanova, C. Deutsch, J. Reichel, and J. G. E. Harris, Phys. Rev. Lett. **112**, 013602 (2014).

[27] F. Y. Khalili, H. Miao, H. Yang, A. H. Safavi-Naeini, O. Painter, and Y. Chen, Phys. Rev. A **86**, 033840 (2012).

[28] D. Lee, M. Underwood, D. Mason, A. B. Shkarin, K. Borkje, S. M. Girvin, and J. G. E. Harris, arXiv:1406.7254.